Molecular dynamics study of chromonics doped with salts

J. P. de Almeida Martins

Under Supervision of Pedro Sebastião and Fabián Vaca Chávez
Mestrado Integrado em Engenharia Física Tecnológica
Instituto Superior Técnico, Lisboa, Portugal

(Dated: June 24, 2014)

In this work we present a Nuclear Magnetic Resonance (NMR) study on the orientational order and molecular dynamics of neat and doped with salts Edicol Sunset Yellow (ESY) solutions. We focus on the nematic and isotropic phases.

^{1}H and ^{23}Na spectra show that the presence of small amounts of NaCl and LiCl induce two effects on the chromonic mesophases: stabilization of the ordered phases and a reduction of the order parameter. These two effects are explained as being a result of two salt-induced competing trends: an elongation of the aggregates and a decrease of their persistence length. Spectroscopy measurements also show that a small and rapid temperature variation causes the bi-phase to undertake a macroscopic phase separation, and that successive heating-cooling cycles increase the order parameter.

Proton NMR relaxometry was used to probe the molecular dynamics of a set of ESY samples with and without additives. In the Nematic phase, the presence of additives seems to contribute to an increase of the strength of the collective motions and a decrease of the self-diffusion coefficient. These effects result from a viscosity increase and an increase of the stacks' flexibility. In the isotropic phase, we observe a decrease of the rotations/reorientations correlation times and a magnitude increase of the collective motions. Both results seem to be caused by an increase of the orientational order.

Keywords: Liquid Crystals, Chromonic, Order Parameter, Nuclear Magnetic Resonance, Relaxation

INTRODUCTION

Unlike common lyotropics, chromonic mesophases are formed through the aggregation of non-amphiphilic molecules which have a plank-like or disk-like polyaromatic central core with polar groups at the periphery [1, 2]. Instead of forming micelles, those molecules stack on top of each other face-to-face to minimize the areas of unfavourable contact with water, leaving the ionic solubilizing groups at the aggregate/water interface. The mesogenic unit of chromonic mesophases are then columns of stacked molecules which lie in a continuum fluid. For certain values of temperature and concentration, the molecular stacks still exist in the Isotropic (I) liquid phase. The most common mesophases in chromonic liquid crystals are the uniaxial Nematic (N) phase and the hexagonal Columnar (C) phase. Between two phases, in a transition from one phase to another, a two-phase state where the initial and final phases coexist is observed. For example, in the process of obtaining the N phase by cooling of an I phase we can observe a N+I state where domains of nematic substance coexist with an isotropic environment.

The N phase is characterized by an arrangement of the stacks along a certain direction defined by a vector $\mathbf{n}$ called director, possessing no long-range positional order. This phase has cylindrical symmetry and has no polarity ($\mathbf{n} = -\mathbf{n}$). To quantify the orientational order of this phase we use the following quantity [3]

$$S = \frac{1}{2}\left\langle 3\cos^2\theta - 1\right\rangle \ . \tag{1}$$

S varies between 1 (completely oriented sample) and 0 (isotropic sample) and is known as the nematic order parameter.

In recent years, increasing attention has been given to chromonics in view of their potential technological applications such as the production of biosensors in the detection of antigens and films with semi-conducting properties (see ref. [4] and references therein). Therefore, the study of their physico-chemical properties is a matter of concern and is currently an active topic of research.

Most studies reported in the literature have been focused on disodium cromoglycate (DSCG), a drug used on the treatment of asthma. However in the last years chromonic phases formed by ESY (whose molecular structure is shown in Fig. 1) have been a subject of both theoretical and experimental studies [5, 6]. Chami and Wilson reported results from molecular dynamics simulations that describe the dynamics and structure of aggregates of ESY molecules. Experimental works made use of techniques such as X-ray, optical microscopy and NMR (^{1}H, ^{2}H and ^{23}Na) spectroscopy [7–9]. Zhou *et al.* measured the temperature and concentration of the Frank elastic constants splay (K_1), twist (K_2), and bend (K_3) [3] using a magnetic Frederiks transition technique in the nematic phase [6].

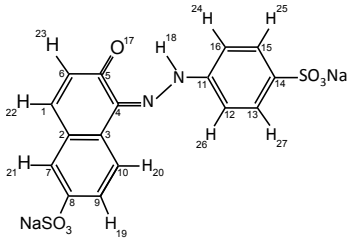

Figure 1: Molecular structure and atom numbering of ESY.

Recently, proton NMR relaxometry and pulse gradient NMR techniques were used to study the molecular dynamics in the chromonic nematic and isotropic phases of the binary mixture composed by Edicol Sunset Yellow and heavy water [10]. Here, we extend that work and we investigate the effect of sodium chloride and lithium chloride on the molecular dynamics of the same chromonic compound.

The works reported in the literature are not just focused on the characterisation of chromonic liquid-crystalline systems formed by aqueous solutions but also on the effect of the addition of salts. Investigation using X-Ray, optical, rheologycal, NMR and dielectric techniques were used to characterise the phase behavior and structure of the mixtures.

Kostko *et al.* investigated the addition of sodium and potassium salts to the nematic phase of DSCG [11]. Park *et al.*, Jones *et al.* and Prasad *et al.* reported the addition of ionic compounds to the aqueous solution of ESY [8, 9, 12].

EXPERIMENTAL DETAILS

Samples Preparation

The objective of this work is to study the effect of salts on the structure and molecular dynamics of ESY's I and N phases. To this end, we prepared three base solutions of ESY and heavy water (D_2O) with concentrations of 30.6 wt%, 27.8 wt% and 26 wt%. In the following, such solutions shall respectively be designated as ESY31, ESY28 and ESY26. The dissolution of ESY in D_2O was done in order to distinguish solvent from solute protons in the NMR measurements. Different amounts of NaCl and LiCl were dissolved in the three base solutions to form the samples ESYx+yz, where x= $\{31, 28, 26\}$, y designates the salt used in the mixture and z is the amount, in molalities, m (1 m = 1 mol/kg), of salt added (e.g.: ESY28+NaCl0.5 designates ESY+D_2O 27.8wt% + LiCl 0.5 m). The samples were placed in standard NMR tubes and flame sealed to avoid water evaporation.

According to the phase diagram present in ref. [7], at room temperature, ESY31 is in the N phase and both ESY28 and ESY26 are in the N+I phase. All the samples were stored at room temperature and no inhomogeneities appeared with time. However, it was detected that heating the ESY28 samples caused them to divide into two coexisting liquid crystalline phases. It must be noted that for the phase separation to take place, it was only necessary to heat the samples 2-5 °C above the room temperature.

Both ESY, NaCl and D_2O with a 99.98 percentage of ^2H atoms were purchased from Sigma-Aldrich (Munich, Germany). LiCl was obtained through Merck Millipore (Darmstadt, Germany). The *chromonic* material was further purified according to the procedure described in [7]. Briefly, the product was dissolved in Milli-Q water with a resistivity higher than $18.2 M\Omega \cdot cm$, followed by addition of ethanol. The dye precipitate was recovered and the process was repeated 4 more times. Finally, the ESY sample was dried in an oven at 60°C to remove residual solvents. The final purity was checked by proton NMR and no traces of impurities were detected. The two other salts as well as D_2O were used without further purification.

NMR measurements

All NMR measurements were performed at Laboratório de Cristais Líquidos e Ressonância Magnética Nuclear at IST. The temperatures at which the measurements were taken were regulated and stabilised with a precision of ±0.4°C using an air current cooled to 1°C by a Julabo f10 refrigerated oilbath.

The ^1H NMR spectra were obtained through a Bruker Avance II 300 spectrometer. Such measurements were performed at a frequency of 300.13 MHz to which corresponds a magnetic field of 7 T. A 90° pulse with a length of 12 μs and a power level of 2 dB was used. The delay time was of 2 s and were taken a total of 32 scans per measurement. A variable-field iron-core magnet equipped with a Bruker Avance II console was used to measure the ^{23}Na NMR spectra. Those spectra were obtained at a frequency of 23.3 MHz, corresponding to a of 2.1 T magnetic field. We used a 90° pulse with a length of 8.05 μs and a power level of 0 dB. The delay time was of 0.5 s and each measurement was formed by a set of 228 scans.

The proton spin-lattice relaxation rate, $R_1(\equiv 1/T_1)$, was measured for almost four Larmor frequency, ν, decades, from 10 kHz to 90.5 MHz. For frequencies higher than 8.9 MHz the measurements were performed using the inversion-recovery technique while for frequencies lower than 8.9 MHz, the fast field-cycling (FFC) technique was used. For the frequency range 9 MHz - 90.5 MHz a variable-field iron-core magnet equipped with a Bruker Avance II console was used. For frequencies below 9 MHz R_1 the data were obtained with a home developed FFC spectrometer [13] operating with both B_P and B_D equal to 0.215 T and a switching time inferior to 3 ms. Time τ was varied between zero and about five times the expected value of the spin-lattice relaxation time.

SPECTROSCOPY

The NMR spectrum of a given sample is defined by the following Hamiltonian [14]

$$\hat{\boldsymbol{\mathcal{H}}} = \hat{\boldsymbol{\mathcal{H}}}_Z + \hat{\boldsymbol{\mathcal{H}}}_{int} \ . \tag{2}$$

The term $\hat{\boldsymbol{\mathcal{H}}}_Z$ consists in the Zeeman Hamiltonian and $\hat{\boldsymbol{\mathcal{H}}}_{int}$ represents the Hamiltonian pertaining to the *internal interactions*. The Zeeman Hamiltonian describes the interaction with an external constant magnetic field $\mathbf{B}_0$ and establishes a set of energy levels completely defined by the spin $\hat{\mathbf{I}}$ of the observed nuclei. The *internal interactions* arise due to mutual influence of the nuclei's electric charges and magnetic moments. A remarkable feature of NMR is that these interactions are usually much weaker than the *external interactions* [14, 15]. Hence, we can treat them as perturbations that shift the energy levels of the spectrum defined by the Zeeman interaction with $\mathbf{B}_0$.

For a spin $I = 1/2$ the dominant internal interaction is the direct interaction between the magnetic dipole moments of two nuclei (Dipolar Coupling). It can be shown that, for an Uniaxial N phase, this interaction results in the following splitting between consecutive energy levels [15]:

$$\Delta\nu_{ij,d} = \frac{3\mu_0}{16\pi^2}\gamma^2\hbar\left(\frac{3\cos^2\phi - 1}{2}\right)\left\langle\frac{3\cos^2\beta_{ij} - 1}{r_{ij}^3}\right\rangle S \ , \tag{3}$$

where S is the order parameter and ϕ is the angle between $\mathbf{n}$ and $\mathbf{B}_0$. r_{ij} is the distance between nuclei i and j. The quantity β_{ij} is the polar angle that defines the position of the inter-nuclear vector in the molecular frame.

The dominant internal interaction for a spin with $I > 1/2$ is the interaction between the nuclei and the involving electronic environment (Quadrupolar Coupling). For an Uniaxial N phase, this interaction causes the following splitting [15]:

$$\Delta\nu_{i,q} = \frac{3}{4}C_{i,Q}\left(\frac{3\cos^2\phi - 1}{2}\right)\left\langle\frac{3}{2}\cos^2\beta_i - \frac{1}{2}\right\rangle S \ . \quad (4)$$

As before, S is the order parameter and ϕ is the angle between $\mathbf{n}$ and the magnetic field. $C_{i,Q}$ is the strength of the electric field gradient felt by the nucleus i and β_i is the polar angle that defines the position of such gradient in the molecular frame.

^{1}H Spectroscopy

Inspection of Fig. 2 shows us that each phase possesses a clearly distinct NMR spectrum. In the I phase (Fig. 2(a)) no splitting is observed and the spectrum consists of various peaks corresponding to the chemical shifts of different ^{1}H. The spectrum of the N phase (Fig. 2(b)) is characterized by the existence of two, almost symmetric, broad peaks caused by the dipolar splitting. The broad nature of such peaks is attributed to the the inter-proton distance. Because all the ^{1}H nucleus have a similar first-neighbour distance (in the 2.44-2.50 Å range [7]), their spectra overlap, causing the observed broadening. When the sample is in the N+I phase (Fig. 2(c)), the observed spectrum consist in an overlapping of the spectra characteristic to the N and I phases.

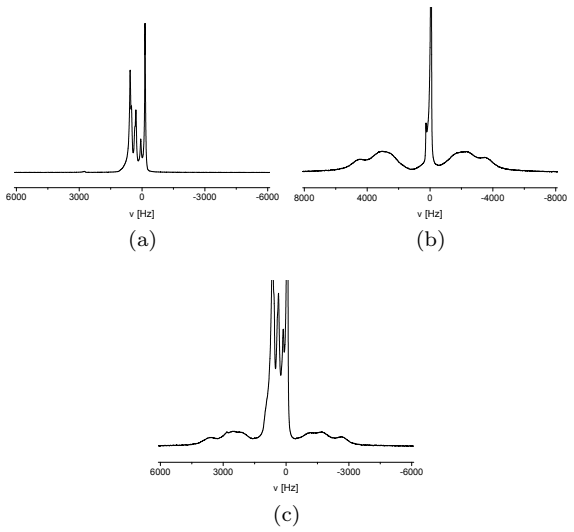

Figure 2: Typical ^{1}H spectra of the I, (a), N, (b), and N+I, (c), phases of ESY.

Due to J-Coupling effects each one of the lateral peaks consists in a combination of two doublets and a triplet. The doublets result from three pairs of protons, one from H_{24}-H_{25} plus H_{26}-H_{27} and another from H_{19}-H_{20}; the triplet is due to H_{21}-H_{22}-H_{23}. Because they overlap, it is difficult to identify and distinguish the doublets. The two outer peaks of the 1:2:1 triplet can however be identified as the two smaller peaks in the extremes of the spectrum. Following the procedure of Edwards *et al.* [7], the $\Delta\nu_d$ values were measured as being half of the separation of those two smaller peaks.

The measured $\Delta\nu_d$ values can be related to the ESY mesophases' orientational order through Eq. (3) with $\phi = 90°$ due to the negative anisotropy of the diamagnetic susceptibility of ESY. Because the measured splitting results from the interaction of H_{22} with both H_{21} and H_{23}, $\Delta\nu_d$ is calculated as an average of the splittings caused by H_{21}-H_{22} and H_{22}-H_{23}. According to Edwards *et al.* [7], the distances of those ^{1}H pairs, $r_{21,22}$ and $r_{22,23}$, have constant values of 2.44 Å and 2.48 Å, respectively. In the same ref. [7] it is also considered that $\beta_{21,22} = \beta_{22,23} = 90°$.

^{23}Na Spectroscopy

As expected, the ^{23}Na spectrum of an ESY sample in the I phase consists in a single Lorentzian distribution. In the N phase, the anisotropy of the electric environment creates a quadrupolar splitting related to the order parameter through Eq. (4). For a sample in a macroscopically aligned state, the N phase spectrum consists of $2I$ equally spaced lines corresponding to the various $m \rightarrow m+1$ transitions, whose intensities are roughly proportional to $I(I+1) - m(m-1)$. In the case of a ^{23}Na spectrum we have three lines with a $3:4:3$ ratio.

As before, the N+I phase spectrum is an overlapping of the N and I phases' spectra. Considering that such spectrum is just a linear combination of a N phase spectrum and an I phase spectrum, we can define the following quantity

$$Q_{\rm iso} = \frac{1}{3}\left(5 - \frac{2}{A_{cp}}\right) \ . \quad (5)$$

where A_{cp} is the central peak area normalized to the total area. The quantity $Q_{\rm iso}$ varies between 1 and 0 and evaluates the quantity of material in the I phase.

To describe the ^{23}Na splitting we resort to the ion condensation model. Developed for the study of counterion binding in polyelectrolytes [16], this model distinguishes between weakly bounded ions, termed as "free", and strongly bound counterions, termed as "bound". The fraction of "bound" ions is considered to be independent of water content, temperature and addition of simple salts [15, 17]. These ions experience a much more intense electric field gradient, making their contribution to $\Delta\nu_q$ is the dominant one. Since the ion condensation model is normally consistent with the assumption of a single binding site [15, 17], Eq. (4) can be approximated by [15, 17]:

$$\Delta\nu_q = p_b\Delta\nu_{b,q} \ , \quad (6)$$

where p_b is the fraction of "bound" counterions and $\Delta\nu_{b,q}$ is the corresponding splitting. Although the number of "bound" counterions is typically consistent with the neutralization of ∼70% of the stacks' charge, the exact value of p_b is not known. Because the value of $C_{i,Q}$ depends on

the detailed structure of the binding site [15], such quantity is also not known. Thus, Eq. (6) cannot be used to calculate S_{zz} and only a qualitative or comparative analysis can be done through it.

Results and Discussion

Analysis of the Phase Separation

As pointed before, by heating a sample of ESY28 one induces a macroscopic phase separation between two phases. This phase separation was visually detected by noting that the heating process caused the sample to divide itself in two regions with distinct colors, as illustrated in Fig. 3(a). The origin of the separation is unclear and, to the author's knowledge, as of yet there are no reports of its existence in pure solutions of ESY.

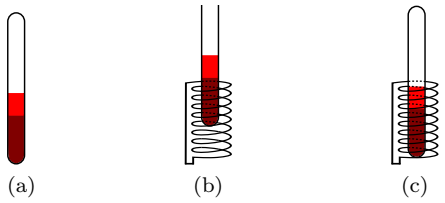

Figure 3: Fig. (a) represents the phase separation of the N+I phase. The darker area corresponds to the more ordered part while the lighter area corresponds to the less ordered part. The difference in colors was exaggerated for clarity. Figs. (b) and (c) illustrate two ways of positioning the phase-separated sample in the NMR coils. In (b) only the ordered part is involved by the coils while in (c) all the material is involved.

To study the phase-separation process, we placed an ESY28 sample in the NMR spectrometer at 25 °C over a period of 140 minutes. During this period the sample was also subjected to a magnetic field of 2.1 T. By measuring a ^{23}Na NMR spectrum every 5 minutes, it was possible to track the time-evolution of the sample's phases. The results of this procedure are present in Fig. 4(a) which shows the time variation of Q_{iso}.

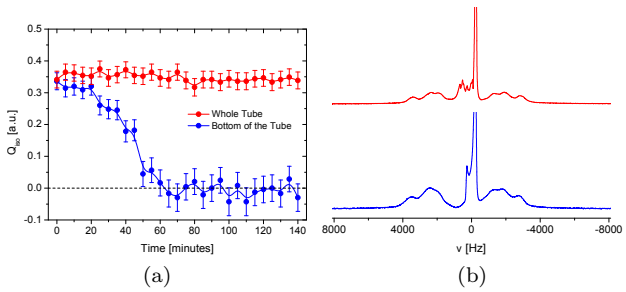

Figure 4: (a), time evolution of the Q_{iso} values during the phase separation process. The two colors represent two ESY28 samples placed in the spectrometer in two distinct ways. (b), ^{1}H spectra of the same samples represented in (a) in their phase-separated state. The two colors have the same meaning as in (a). See text for details.

The different colors in Fig. 4(a) identify two distinct samples, placed in the spectrometer in different ways. Both samples were not previously submitted to any measuring or heating event of any kind. Samples with such history shall henceforth be referred to as *fresh*. The data in blue was obtained for a sample positioned in a way where only its bottom part was involved by the detection coils (see Fig. 3(b)). The points in red describe the totality of the material present in the NMR tube (see Fig. 3(c)). The blue data decreases monotonically until it reaches a point compatible with $Q_{\text{iso}} = 0$, after which it stays constant within the experimental uncertainty. This evolution shows that the bottom part of the sample condenses into a N phase after, approximately, 1 hour. On the other hand, the red data stays approximately constant for the entire duration of the experiment. Thus, the phase separation process does not alter the total quantity of ordered material. The identification of the two phases as a N+I (all tube) and N (bottom of the tube) was confirmed via ^{1}H spectroscopy (see Fig. 4(b)).

While performing the aforementioned experiments, we detected no variations of quadrupolar splitting. Both the bottom part and the whole sample kept a constant $\Delta\nu_q$ during the demixing process. This fact shows that, despite the increase in ordered material at the bottom of the tube, the degree of order is not affected by the phase-separation.

The repetition of the above experience for an ESY31 sample in the N+I phase wielded the same results. In a separate experiment an ESY28 sample was left in a thermal bath at 25 °C for 140 minutes. No magnetic field of any kind was applied to the sample before the NMR measurements. Since the results of this experience were consistent with the ones where the sample was placed in a magnetic field, we see that the field does not influence the phase separation.

The above results indicate that the N+I phase is metastable, being destroyed by a heating process. The destruction of the homogeneous biphasic state is caused by a nucleation process where increasingly larger droplets of ordered material are formed [18]. Because the N material has a higher density, after a certain critical size the droplets suffer a gravity-induced flow to the bottom of the tube, thus explaining the observed phase-separation.

To study the variation of the quadrupolar or dipolar splittings with temperature, the typical procedure is to heat the samples until the I phase is achieved, and to perform the measurements while reducing the temperature. After a temperature cycle where proton spectra were acquired, we noticed that the splitting at room temperature was greater than the value recorded before heating the sample. To study this effect in more detail we submitted a *fresh* sample of ESY28 to various temperature cycles and measured its ^{23}Na NMR spectra during such cycles. In Fig. 5 we can see the evolution of $\Delta\nu_q$ with those cycles.

Inspection of Fig. 5 shows that the quadrupolar splitting increases with the number of cycles until saturation is achieved at the fourth cycle. A sample whose splitting no longer presents a significant dependence on the temperature cycles is denoted as "saturated". The phase transitions temperatures were determined from Q_{iso} within an error of 1.25 °C. It appears that the number of cycles influences the temperature of the I → N+I transition but not the temperature of the N+I → N transition.

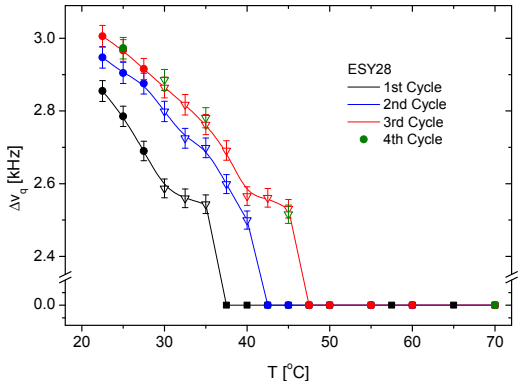

Figure 5: Evolution of the Quadrupolar Splittings, (a), and $Q_{\rm iso}$ values, (b), of ESY28 with the number of temperature cycles. The full circles represent a N phase, the open triangles a N+I phase and the full squares an I phase.

Addition of salts

Fig. 6 shows the ^{1}H and ^{23}Na spectra of ESY28, ESY28+NaCl0.5 and ESY28+LiCl0.5. All the spectra correspond to a N phase.

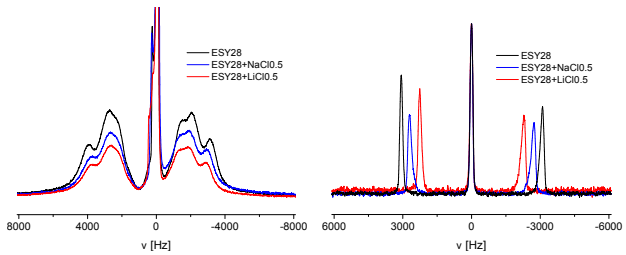

Figure 6: ^{1}H, (a), and ^{23}Na, (b), spectra of ESY28, ESY28+NaCl0.5 and ESY28+LiCl0.5. The different intensities of distinct ^{1}H spectra were artificially created to highlight the differences in the splittings.

It is seen that the addition of NaCl or LiCl causes a reduction of the dipolar and quadrupolar splittings. According to Eq. (3), the decrease in $\Delta\nu_d$ results from a decrease in orientational order. The decrease in $\Delta\nu_q$ is also consistent with a reduction of the order parameter.

The similar values of $\Delta\nu_d$ of ESY28+NaCl0.5 and ESY28+LiCl0.5 indicate that the two salts have a similar effect on the orientational order of ESY28. Thus, the fact that the quadrupolar splitting of ESY28+LiCl0.5 is smaller than the quadrupolar splitting of ESY28+NaCl0.5 is rather remarkable as both samples appear to have the same value of S_{zz}. It is possible that the Li^+ ions, smaller than the Na^+ counterions, may penetrate through the layer of "bound" Na^+. This process would cause a displacement of the sodium ions, with the Li^+ ions assuming the old positions of the "bound" Na^+ ions. Such behaviour may lower the strength of the quadrupole coupling due to effects of shielding or even reduce the number of "bound" sodium ions, thus explaining the smaller ^{23}Na splitting of ESY28+LiCl0.5.

We now focus on the variation of orientational order with temperature. In Fig. 7 we can see the effect of temperature on the ^{1}H and ^{23}Na splittings of an ESY28 sample. Those spectra were obtained for a *saturated* sample which, at $\sim 25\,^{\circ}$C, was positioned according to Fig. 3(b). All the points in Fig. 7 were taken on cooling.

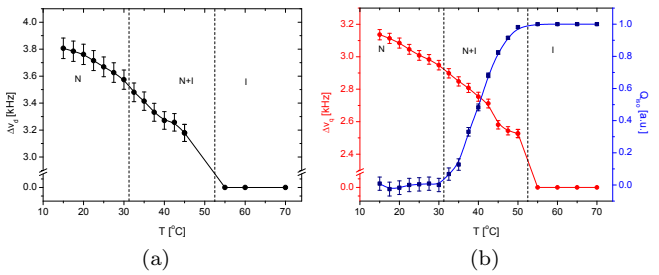

Figure 7: Variation of the Dipolar, (a), and Quadrupolar, (b), splittings of ESY28 with the temperature. The points were taken on cooling.

Figs. 7(a) and 7(b) show that both splittings decrease slightly with a temperature increase. The variation of $\Delta\nu_q$ with temperature is similar to the variation of $\Delta\nu_d$, which reinforces the validity of the ion condensation model and suggests that the variation is created by small changes in aggregate ordering. Another noticeable feature of Fig. 7 are the high phase transition temperatures, which are incompatible with the ones reported in ref. [7]. The higher transition temperatures are explained by the positioning of the sample, which focus the analysis on the ordered material at the bottom of the phase separated state.

The data showed in Fig. 7 was fitted to the Haller approximation [19]:

$$S_{zz}(T) \equiv S(T) = S_0 \left(1 - \frac{T}{T_c}\right)^{\beta} , \qquad (7)$$

where S_0 is a constant scaling factor and β is a material constant. T_c is the temperature, in Kelvins, at which the studied material changes phase. The fits were performed by considering the points belonging to a N phase and the points of the N+I phase with $Q_{\rm iso} \leq 0.5$. The considered phase transition was the I→N+I one, $T_c = T_{\rm I\to N+I}$. This procedure simulates the behaviour of a *thermotropic* nematic and facilitates the comparison with that type of liquid crystals.

The splittings from the ^{1}H and ^{23}Na spectra of ESY28 were simultaneously fitted to Eq. (7) considering a common exponent β. In such fit, the temperatures $T_c = T_{\rm I\to N+I}$ were fixed to our measurements. This procedure resulted in $\beta = 0.12 \pm 0.07$, a value slightly smaller than the ones obtained for typical thermotropic liquid crystals, $\beta = 0.16 - 0.19$ [20]. The smaller exponent indicates that the orientational order of chromonics depends less on the temperature.

Fig. 8 simultaneously displays the temperature-evolution of the ^{23}Na splitting of ESY28, ESY28+NaCl0.5 and ESY28+LiCl0.5. The displayed data corresponds to *saturated* samples which, at $\sim 25°$C, were positioned according to Fig. 3(b). All the spectra were measured on cooling.

Inspection of Fig. 8 reveals that the samples with salts present the same qualitative features as ESY28, namely, a small variation with temperature. As before, we fitted the data to Eq. (7) to analyse their temperature. Such fits wielded $\beta = (1.51 \pm 0.08) \times 10^{-1}$ and $\beta = (1.46 \pm 0.09) \times 10^{-1}$ for ESY28+NaCl0.5 and

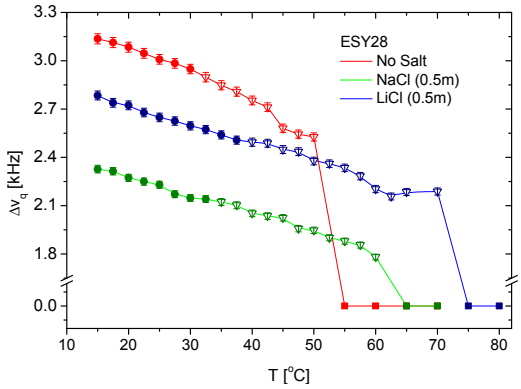

Figure 8: Comparison between the Quadrupolar Splittings, (a), and $Q_{\rm iso}$ values, (b), of ESY28, ESY28+NaCl0.5 and ESY28+LiCl0.5. The full circles represent a N phase, the open triangles a N+I phase and the full squares an I phase.

ESY28+LiCl0.5, respectively. Since the exponents for the salted solutions are higher than the unsalted one, it appears that the presence of additives increases the temperature dependence of the order parameter.

Fig. 8 shows that the addition of NaCl or LiCl increases the phase transition temperatures. The same figure also shows a salt-induced reduction of $\Delta\nu_q$ consistent with our previous discussion. It appears that the NaCl and LiCl have two seemingly inconsistent effects: a stabilization of the ordered phases and a reduction of the degree of order, represented by the order parameter. To better understand this effect we discuss in some detail the effects of the salts in the mesophases structure.

The main effect of ionic additives on polyelectrolyte solutions is the screening of electrostatic repulsive forces. In the case of ESY solutions, there are two types of electrostatic repulsions, those who act between molecules of the same stack and those who act between molecules of different stacks. In ref. [21] it is proposed that the salt-induced screening of electrostatic repulsions increases the aggregates' length, L, and enhances their flexibility. The increase in flexibility is equivalent to a shortening of the persistence length l, the characteristic distance between two different parts of the aggregate that are correlated.

The increase of L and the decrease of l induce two competing effects on the orientational order; while the former promotes it, the latter represses it. We then have two opposing trends whose interplay may explain the salt-induced reduction of the order parameter and the salt-induced increase of the phase transition temperatures. The effects of varying the aforementioned lengths on the chromonic's phase diagram was analysed using the model developed by Khokhlov and Semenov for semiflexible polymers [22]. According to such model, an increase of L coupled with a decrease of L may only cause the experimentally observed effects if the aggregates are rigid ($L/l \ll 1$).

Transposing the previous ideas to the ESY aggregates, it is suggested that the stacks are rigid entities who are elongated and turned more flexible by the addition of salts. The elongation turns the ordered phases more stable due to excluded volume effects while the higher flexibility reduces the order parameter due to a loss of correlation that creates several independent angles θ along the aggregates, thus affecting the average in Eq. (1). It must be noted that our observations paint a more dynamical picture than the one laid down by Park *et al.*. In ref. [21] it is proposed that the opposing trends result in two concentration dependent zones: for higher concentrations of ESY the salts suppress the orientational order and for lower concentrations of ESY the salts promote it. However, our measurements show that, even for low concentrations, the orientational order is, to some extent, destroyed as the order parameter is lowered.

RELAXOMETRY

Relaxation Mechanisms and Models

Based on the assumption that the molecular motions present in a liquid crystal are statically independent or otherwise are characterised by distinct correlation times, the experimental relaxation rate R_1 is usually assumed to be described by a linear combination of relaxation contributions, each one associated with a specific type of motion. Cross-terms can be neglected as the characteristic correlation times associated with those motions are usually considerably different. Then, the total relaxation rate can be expressed as

$$R_1 = R_{1,\rm C} + R_{1,\rm IM} \tag{8}$$

where C and IM refer to *collective motions* and *individual molecular motions*, respectively.

Here, we summarise the relaxations models used to describe the results. More details can be found in refs. [23, 24].

Individual Molecular Motions

Individual molecular motions can be separated in: molecular rotations and translation displacements of molecules by diffusion processes. To describe the rotations we used the Woessner model [24, 25] while for the translation motions we used the model proposed by Torrey [24, 26] for isotropic liquids.

The model proposed by Woessner considers the relaxation induced by reorientations of rigid elongated molecules. This model accounts for the anisotropic nature of a certain molecule by considering rotations along two different axes. The spectral densities are given by:

$$J_k(\nu) = \frac{4}{3} c_k \sum_{m=-2}^{2} \frac{\overline{|d^2_{k0}(\beta_{ij})|^2}}{r^6_{ij}} \langle |D^2_{km}(\theta)| \rangle \frac{\tau_{|m|}}{1 + 4\pi^2\nu^2\tau^2_{|m|}} \ , \tag{9}$$

where r_{ij} are the inter-proton distance ($\sim$2.5Å for the first neighbours of an ESY molecule, according to ref. [7]) and β_{ij} denotes the angle between the inter-proton vector and the long molecular axis. D^2_{km} is the second rank Wigner rotation matrix and the averages $\langle |D^2_{km}(\theta)| \rangle$ can be expressed in terms of the second and fourth rank Legendre polynomials of the angle between the long molecular axis and the nematic director [24]. $d^2_{km}(\beta_{ij})$ is the second rank reduced Wigner rotation matrix.

The correlation times, $\tau_{|m|}$, can be expressed as $\tau_0 = \tau_s$, $\tau_1 = (\tau_s^{-1} + \tau_f^{-1})^{-1}$, and $\tau_2 = (\tau_s^{-1} + 4\tau_f^{-1})^{-1}$. τ_f and

τ_s are two distinct correlation times that usually correspond to molecular reorientations about an axis parallel and perpendicular to the long molecular axis, respectively. In the present work, the times τ_f and τ_s correspond to reorientations parallel and perpendicular to the packing axis.

According to the Torrey model the relaxation rate can be written as:

$$\left(\frac{1}{T_1}\right)_{\text{Diff}} = C_D \frac{n\tau_D}{d^3}\left[\mathcal{J}(\nu)) \; + \; 4\mathcal{J}(2\nu)\right] \; , \qquad (10)$$

where the dimensionless spectral density $\mathcal{J}(\nu)$ can be calculated analytically [23]. C_D is the magnitude of the dipolar interaction, τ_D is the average time between diffusion jumps, d is the molecular width, n is the density of ^{1}H spins. The mean-square jump distance $\langle r^2 \rangle$ is related with the self-diffusion constant D and τ_D by the relation $\langle r^2 \rangle = 6\tau_D D$ [23, 24].

Collective Motions

In the nematic phases of thermotropic and lyotropic liquid crystals the collective motions are fluctuations of the director in three orthogonal directions and are known as Order Director Fluctuations (ODF). However, considering that the mesogenic units of a chromonic nematic phase are molecular stacks, it was shown that the collective motions of such phases are described by Elastic Column Deformations (ECD) [10]. The corresponding spectral density is [27]

$$J_{\text{ECD}}(\nu) = \frac{kT\eta}{2\pi^2}\int_{q_{\perp,\text{l}}}^{q_{\perp,\text{h}}}\int_{q_{||,\text{l}}}^{q_{||,\text{h}}} dq_\perp \, dq_{||} \times \\ \times \frac{q_\perp \, q_{||}^4}{(2\pi\nu)^2\eta^2 q_{||}^4 + (K_3 q_{||}^4 + B q_\perp^2)^2} \; . \qquad (11)$$

η is an average effective viscosity and the quantities $q_{\perp,\text{h}}$ and $q_{||,\text{h}}$ are the components of the largest wave vectors of the deformation parallel and perpendicular to the columns, respectively. The shortest wave vectors are $q_{\perp,\text{l}}$ and $q_{||,\text{l}}$. High and low cut-off frequencies can be defined in terms of the limit wave vectors and the viscoelastic constants.

Close to the temperature of the I→N transition, short-range nematic order can be found in the I phase. Fluctuations of that local order, known as Order Parameter Fluctuations (OPF), can contribute to the spin-lattice relaxation. The resulting spectral density is [23, 28]:

$$J_{\text{OPF}}(\nu) = A_{\text{OPF}} \int_{x_{\min}}^{x_{\max}} \frac{\sqrt{x}\; dx}{(2\pi\nu)^2 + \left(x + \tau_0^{-1}\right)^2} \; , \qquad (12)$$

with $\tau_0 = \nu\xi^2/L$, where ν is an average effective viscosity and ξ is the coherence length of the fluctuations. The limits in the integral are related to the minimum and the maximum wave vectors and A_{OPF} is a constant related with the viscoelastic properties of the liquid crystal in the isotropic phase. In ref. [10], it was shown that OPF contribute significantly to the spin-lattice relaxation of ESY in the I phase.

Results and Discussions

Nematic phase

The Nuclear Magnetic Relaxation Dispersion (NMRD) profiles for the samples ESY28, ESY28+NaCl0.5 and ESY28+LiCl0.5 at 15 °C are displayed in Fig. 9. Such temperature corresponds to the N phase for all the samples. The inset of the same figure displays the NMRD profiles of ESY28 and of the ESY+D_2O solution at 30 wt% (ESY30) analysed in [10]. The ESY28 profile was obtained at 15 °C and the ESY30 profile was obtained at 23 °C; both temperatures correspond to a N phase.

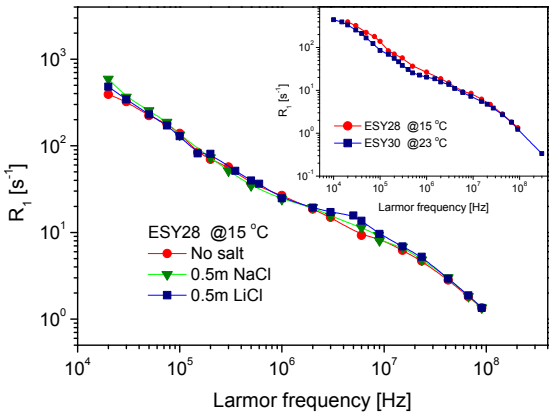

Figure 9: NMRD profiles of ESY28, ESY28+NaCl0.5 and ESY28+LiCl0.5 in the N phase at 15 °C. The inset shows the NMRD profiles of ESY28 and ESY30 in the N phase at 15 °C and 23 °C, respectively. Solid lines are guides for the eyes

Comparison of the two profiles displayed in the inset of Fig. 9 shows that they possess a qualitatively similar behaviour. Despite the similarities between the NMRD profiles of ESY28 and ESY30, they have some differences at intermediate and low frequencies ($\lesssim$ 10 MHz); at high frequencies the two profiles look identical.

The NMRD profiles showed in Fig. 9 present a rather small dependence on the presence of the salts. In fact, at high frequencies the data sets overlap. The minor differences are observed at intermediate frequencies (1-10 MHz) and at low frequencies (below 50 kHz). Despite the small differences in the the NMRD profiles, the ^{1}H spectra of the same samples clearly shows a reduction of orientational order induced by the addition of salts.

In order to interpret the R_1, a fit was performed using Eq. (8) and a home written minimization software package [29]. For a detailed analysis the two individual motions contributions in $R_{1,\text{IM}}$ are shown separately. Based on the fact that the profiles of ESY28 and ESY30 coincide at high frequencies, the fit of the former was carried out by fixing the value of τ_f to the corresponding one of ESY30 at 23 ^{o}C from ref. [10]. Also, the self-diffusion coefficient was extracted from the same work as an extrapolation to 15^{o}C. The fitted experimental data are presented in Fig. 10 together with the separate contributions of the proposed dynamic mechanisms to the total R_1.

The results of the fitting parameters are displayed in Table I, where A_{ECD} corresponds to the magnitude of the ECD model and is related to the sample's viscoelastic

properties, $A_{\rm ECD} \propto \eta/(B\,K_3)$. The errors displayed in all the tables of this chapter are not the typical fitting errors. Due to the inter-dependence of the fitting parameters, their errors have a magnitude much higher than it would be physically expected. To estimate the error of a certain fitting parameter, we performed fits where only that one parameter was left as free in order to estimate its fitting error. Such procedure allows us to analyse the impact of a specific fitting parameter to the global fitting quality within a $\sim 68\%$ confidence level [30].

Table I: Details of the fitting parameters according to the proposed models to describe the frequency dependence of R_1 for the samples ESY28, ESY28+NaCl0.5 and ESY28+LiCl0.5 in the nematic phase at 15 °C. * Fixed from [10]. The values between parenthesis were obtained when those parameters were included in the fit (see text for details).

	ESY28	ESY28+NaCl0.5	ESY28+LiCl0.5
τ_f [$\times 10^{-9}$ s]	1.2* (1.2 ± 0.2)	1.9 ± 0.4	1.6 ± 0.3
τ_s [$\times 10^{-9}$ s]	4.1 ± 0.5	6.2 ± 0.2	4.7 ± 0.5
$A_{\rm ECD}$ [$\times 10^3$ s^{-2}]	13.5 ± 0.6	96 ± 5	338 ± 17
D [$\times 10^{-13}$ m^2/s]	5.5* (5.5 ± 0.7)	4.7 ± 0.6	4.3 ± 0.6
ξ [$\times 10^{-9}$ m]	1.2 ± 3	0.9 ± 1.3	0.8 ± 0.5
S	0.59	0.56	0.56

From the cut-off frequencies associated to ECD we can estimate the ratio $\sqrt{\omega_{\rm hc}/\omega_{\rm lc}} = \xi/\ell$. ℓ and ξ are, respectively, the smallest and largest domains where coherent motions occur. In the case of ESY, ℓ is equal to the stacking distance. Using ξ as a fitting parameter we estimate a coherence length compatible with stacks of 5 ± 2, 3 ± 2 and 4 ± 1 molecules for ESY28, ESY28+NaCl0.5 and ESY28+LiCl0.5, respectively. Those values are consistent with the aggregation number of 11 molecules reported by Park et al. [8], and with the values reported by Cachitas *et al.* [10].

The fact that only a few molecules are involved in the collective motion indicates that this type of movements involves a correlation between molecules of the same mesogenic unit, instead of correlations between mesogenic units. This behaviour is clearly different from the collective motions of a typical *thermotropic* liquid crystal, which consist of correlations between mesogenic units.

Our fits show the same features as the ones reported in ref. [10]. Namely, collective motions composed of correlated movements within the stacks and individual motions composed of intra-stack translation diffusion processes and anisotropic reorientations. Reorientations along the stacking axis were found to be faster than reorientations perpendicular to it.

The decrease of the self-diffusion coefficient in the samples with salt agrees with the finding of an increase of the viscosity of the ESY solutions with the addition of salts reported by Prasad *et al.* [12]. A salt-induced increase of the correlation times for the rotations/reorientations is also observed. The fact that ESY28+NaCl0.5 and ESY28+LiCl0.5 have different times τ_s might be related with the differences between the two ions in the equilibrium and stabilisation of the ESY stacks.

As seen before, the addition of salts decrease the coherence length ξ. Another effect of the salts on the ECD is an increase of $A_{\rm ECD}$. The decrease of both the coherence length and the elastic constants, suggests an increase of the stacks' flexibility with the addition of salts. A higher flexibility leads to a diminution of the free energy needed to distort the stacks and may reduce the coherent molecular motion to smaller domains, thus explaining our observations. This picture is consistent with the discussion present in ref. [21], where it is argued that the addition of salts may lead to a reduction of the aggregates' persistence length. In ref. [31], Zhou *et al.* report a decrease of K_3 caused by the addition of NaCl to an ESY solution, a fact that also supports our analysis.

Isotropic phase

Fig. 11 displays the R_1 dispersion profiles of ESY26, ESY26+NaCl0.5 and ESY26+LiCl0.5 at 50 °C. The inset of that figure shows the NMRD profiles of the ESY26 sample and the ESY+D_2O solution at 24 wt% (ESY24) analysed in [10]. All the samples represented in the inset are in the I phase. It can be observed that the spin-lattice relaxation profile of ESY26 is very similar to the one of ESY24 at 43 °C. ^{1}H NMR spectra of ESY26, ESY26+NaCl0.5 and ESY26+LiCl0.5 show that, at 50 °C, the addition of salts causes the sample to undergo a phase transition from an I phase into a N+I phase. The quantity of nematic material is however so low ($\sim 1\%$), that both ESY26+NaCl0.5 and ESY26+LiCl0.5 will be treated as being in an I phase.

Contrary to the N phase, the NMRD profiles of the I phase are clearly affected by the presence of salts. For frequencies below 1 MHz, the solutions with salts have significantly higher values of R_1 than ESY26; in the interval 1-10 MHz, we can also observe some differences. Above 10 MHZ, the profiles are identical within the experimental uncertainty of $\pm$ 5%.

In Fig.12 are presented the fits performed using model Eq. (8) and considering the presence of OPF. Since the self-diffusion relaxation mechanism presents a small contribution to the relaxation, the value of the self-diffusion constant was fixed to that measured for ESY24 at 43 °C in ref. [10]. As the R_1 profiles in the high frequency regime are similar, it is reasonable to consider that the fast molecular motions in the three samples are characterised by similar correlation times. In fact, very good fits were obtained using the same correlation time τ_f.

The fitting parameters are presented in Table II. Once again, the errors are not the fitting errors, but estimates made by fitting the data with the other parameters fixed.

Both OPF and molecular rotations provide significant contributions to the fit. The first relaxation mechanism is the most important one at lower frequencies (<800 kHz), the second mechanism dominates the high frequencies domain. These characteristics are consistent with the ones reported in ref. [10].

The effect of the presence of salts in the molecular dynamics are observed at frequencies below 10 MHz. Such region is where order parameter fluctuations and reorientation of the molecules about an axis perpendicular to the stacks' axis most affect the relaxation dispersion. Accordingly, inspection of Table II shows us that the ad-

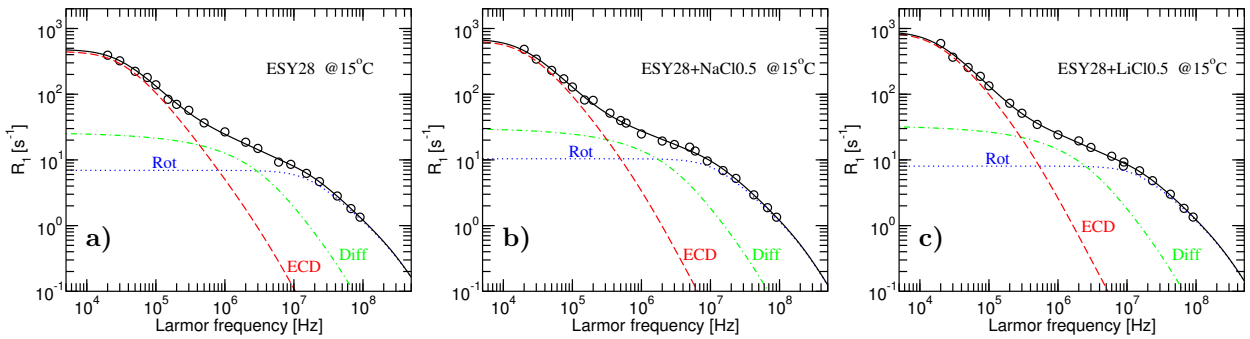

Figure 10: Fits of the R_1 dispersion of ESY28, (a), ESY28+NaCl0.5, (b), and ESY28+LiCl0.5, (c), in the N phase at 15 °C. The solid black curves correspond to the total fitting curves given by Eq. (8) and the dashed coloured curves represent the separate contributions of the proposed dynamic mechanisms. See text for details.

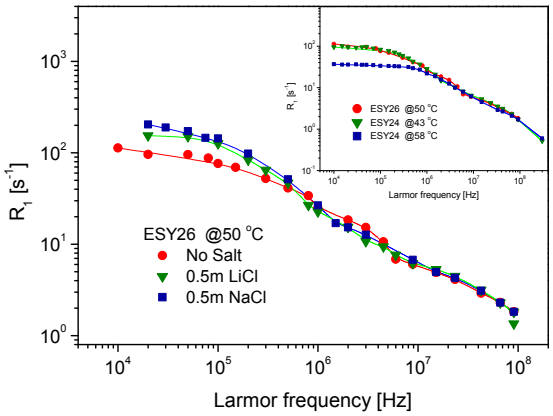

Figure 11: NMRD profiles of ESY26, ESY26+NaCl0.5 and ESY26+LiCl0.5 in the I phase at 50 °C. The inset shows the NMRD profiles of ESY26 at 50 °C, and ESY24 at 43 °C and 58 °C. All the data corresponds to an I phase. Solid lines are guides for the eyes

Table II: Details of the fitting parameters according to the proposed models to describe the frequency dependence of R_1 for the samples ESY26, ESY26+NaCl0.5 and ESY26+LiCl0.5 in the isotropic phase at 50 °C. * Fixed from [10]. The values between parenthesis were obtained when those parameters were included in the fit (see text for details).

	ESY26	ESY26+NaCl0.5	ESY26+LiCl0.5
τ_f [$\times 10^{-9}$ s]	2.5* (2.5 ± 0.2)	2.5* (2.5 ± 0.2)	2.5* (2.5 ± 0.2)
τ_s [$\times 10^{-8}$ s]	4.4 ± 0.4	2.4 ± 0.4	2.6 ± 0.4
A_{OPF} [$\times 10^5$ s^{-2}]	435 ± 24	769 ± 33	533 ± 27

dition of salts causes an increase of A_{OPF} and a decrease of the correlation time τ_s.

Comparing the times τ_s of the ESY28 and ESY26 sample, we find that the correlation time of ESY26 is, approximately, 10× higher than the one of ESY28. We thus see that, for ESY, an increase of orientational order leads to a decrease of τ_s. Then, the lower times of ESY26+NaCl0.5 and ESY26+LiCl0.5 may be caused by an increase of a local orientational order. This argument is in agreement with the increase of the strength of OPF and the ^{1}H spectra of our samples. The same argument can be applied to the N phase and be used to explain the increase of τ_s via the diminution of order observed through ^{1}H spectroscopy.

CONCLUSIONS

It is presented a NMR study of a set of ESY solutions with differing concentrations covering the Nematic (N), Isotropic (I) and biphasic (N+I) phases. Additional samples were prepared by adding 0.5 mol/kg of NaCl and LiCl salts in order to understand the effects of the presence of the additional Na^+ and Li^+ ions in the system. ^{1}H and ^{23}Na NMR spectroscopy were used to measure the temperature dependence of the orientational order of the neat and doped with salts ESY samples. Proton NMR relaxometry was used to probe the molecular dynamics of the N and I phases of the samples.

It was observed that a slight temperature variation caused the N+I phase to separate itself into two distinct macroscopic domains. Spectroscopy measurements showed that the phase separation does not affect the order parameter and identified the more ordered domain as being a N phase. This behaviour was found to be an intrinsic property of the biphasic state caused by its metastability. It was also found that successive heating-cooling cycles increase the orientational order of the mesophases.

^{1}H and ^{23}Na spectra showed that the presence of small amounts of NaCl and LiCl induce two effects on the chromonic mesophases of ESY28: stabilization of the ordered phases, evidenced by an increase of the N+I→N and I→N+I transition temperatures, and reduction of the amount of order, evidenced by a decrease in the dipolar and quadrupolar splittings. No major differences were observed between the samples doped with NaCl and the samples doped with LiCl. However, there are evidences that the extra cations introduced by LiCl displace the sodium counterions of the ESY molecules. The effects of the salts were interpreted as being a result of a salt-induced elongation of the aggregates and a salt-induced increase of the aggregates' flexibility.

The relaxometry results presented here both complement and confirm the ones obtained by Cachitas *et al.* [10]. Once again, the collective motions of the N phase were found to be composed of fluctuations within the mesogenic units instead of fluctuations of the mesogenic units themselves. This distinguishes the dynamics of ESY from the dynamics of typical *thermotropic* liquid crystals.

In the N phase, the addition of NaCl and LiCl to ESY systems contributed to a modification of the reorientation of the molecules, an increase in the self-diffusion constant and to an increase of the strength of the collective mo-

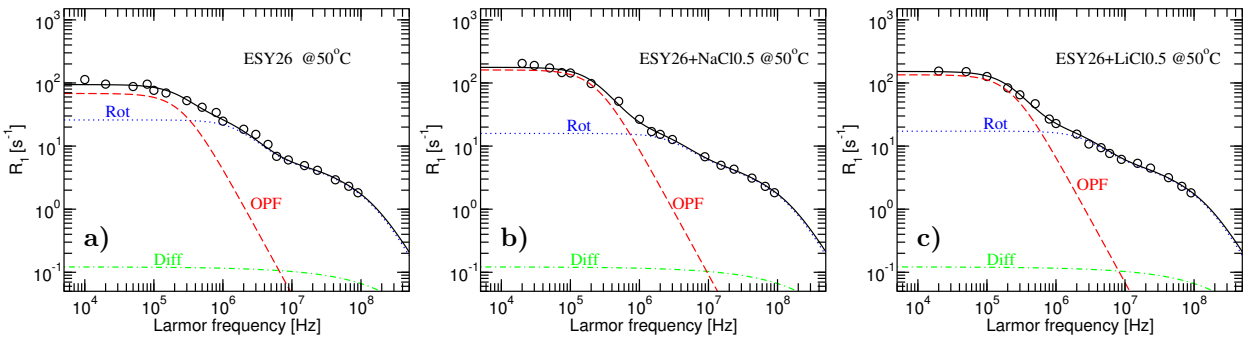

Figure 12: Fits of the R_1 dispersion of ESY26, (a), ESY26+NaCl0.5, (b), and ESY26+LiCl0.5, (c), in the I phase at 50 °C. The solid black curves correspond to the total fitting curves given by Eq. (8) and the dashed coloured curves represent the separate contributions of the proposed dynamic mechanisms. See text for details.

tions. The first one of these effects was explained by a decrease of orientational order while the second was seen as a consequence of a viscosity increase. Besides increasing in magnitude, the collective motions were also seen to involve fewer molecules upon the addition of salts. In agreement with the spectroscopy results, these two observations seem to indicate a salt-induced increase of the flexibility of the aggregates. The effects of the ionic additives were more visible in the I phase. Here, the salts also affected the molecular rotations/reorientations and increased the strength of the collective motions. Both results were interpreted as being caused by an augment of the local order which was also observed in ^{1}H spectra.

[1] J. Lydon, Liq. Cryst. **38**, 1663 (2011).

[2] P. Collings, A. Dickinson, and E. Smith, Liquid Crystals **37**, 701 (2010).

[3] P. G. de Gennes and J. Prost, *The Physics of Liquid Crystals*, International Series of Monographs on Physics (Clarendon Press, 1995).

[4] H.-S. Park and O. D. Lavrentovich, "Liquid crystals beyond displays: Chemistry, physics, and applications," in *Liquid Crystals Beyond Displays*, edited by Q. Li (John Wiley & Sons, Inc., 2012) Chap. Lyotropic Chromonic Liquid Crystals: Emerging Applications, pp. 449–484.

[5] F. Chami and M. R. Wilson, Journal of the American Chemical Society **132**, 7794 (2010).

[6] S. Zhou, Y. A. Nastishin, M. M. Omelchenko, L. Tortora, V. G. Nazarenko, O. P. Boiko, T. Ostapenko, T. Hu, C. C. Almasan, S. N. Sprunt, J. T. Gleeson, and O. D. Lavrentovich, Phys. Rev. Lett. **109**, 037801 (2012).

[7] D. Edwards, J. Jones, O. Lozman, A. Ormerod, M. Sintyureva, and G. Tiddy, The Journal of Physical Chemistry B **112**, 14628 (2008).

[8] H.-S. Park, S.-W. Kang, L. Tortora, Y. Nastishin, D. Finotello, S. Kumar, and O. D. Lavrentovich, The Journal of Physical Chemistry B **112**, 16307 (2008).

[9] J. Jones, L. Lue, A. Ormerod, and G. Tiddy, Liquid Crystals **37**, 711 (2010).

[10] H. Cachitas, P. J. Sebastião, G. Feio, and F. Vaca Chávez, Liquid Crystals **41**, 1080 (2014).

[11] A. F. Kostko, B. H. Cipriano, O. A. Pinchuk, L. Ziserman, M. A. Anisimov, D. Danino, and S. R. Raghavan, The Journal of Physical Chemistry B **109**, 19126 (2005), pMID: 16853466.

[12] S. K. Prasad, G. G. Nair, G. Hegde, and V. Jayalakshmi, *The Journal of Physical Chemistry B*, J. Phys. Chem. B **111**, 9741 (2007).

[13] D. M. Sousa, G. D. Marques, J. M. Cascais, and P. J. Sebastião, Solid State Nuclear Magnetic Resonance **38**, 36 (2010).

[14] C. Slichter, *Principles of Magnetic Resonance*, Lecture Notes in Computer Science (World Publishing Company, 1990).

[15] J. Emsley, *Nuclear magnetic resonance of liquid crystals*, NATO ASI series: Mathematical and physical sciences (Published in cooperation with NATO Scientific Affairs Division [by] D. Reidel Pub. Co., 1985).

[16] G. S. Manning, Annual Review of Physical Chemistry **23**, 117 (1972).

[17] H. Wennerström, B. Lindman, G. Lindblom, and G. J. T. Tiddy, J. Chem. Soc., Faraday Trans. 1 **75**, 663 (1979).

[18] N. Goldenfeld, *Lectures on Phase Transitions and the Renormalization Group*, Advanced Book Program (Addison-Wesley, Advanced Book Program, 1992).

[19] I. Haller, Progress in Solid State Chemistry **10, Part 2**, 103 (1975).

[20] I. Chirtoc, M. Chirtoc, C. Glorieux, and J. Thoen, Liquid Crystals **31**, 229 (2004).

[21] H.-S. Park, S.-W. Kang, L. Tortora, S. Kumar, and O. D. Lavrentovich, Langmuir **27**, 4164 (2011).

[22] A. Khokhlov and A. Semenov, Physica A: Statistical Mechanics and its Applications **112**, 605 (1982).

[23] R. Dong, *Nuclear magnetic resonance of liquid crystals*, Partially Ordered Systems Series (Springer-Verlag Gmbh, 1997).

[24] P. J. Sebastião, C. Cruz, and A. C. Ribeiro, in *Nuclear Magnetic Resonance Spectroscopy of Liquid Crystals*, edited by R. Y. Dong (World Scientific, Singapore, 2010) pp. 129–167.

[25] D. E. Woessner, J. Chem. Phys. **36**, 1 (1962).

[26] H. C. Torrey, Phys. Rev. **92**, 962 (1953).

[27] S. Žumer and M. Vilfan, Molecular Crystals and Liquid Crystals **70**, 39 (1981).

[28] Vaca Chávez, F. and Sebastião, P. J. and Miyake, Y. and Monobe, H. and Shimizu, Y., *The Journal of Physical Chemistry B*, J. Phys. Chem. B **116**, 2339 (2012).

[29] P. J. Sebastião, Eur. J. Phys. **35**, 015017 (2014).

[30] F. James and M. Roos, CERN Program Library Long Writeup **D506** (1994).

[31] S. Zhou, A. J. Cervenka, Y. Singh, L. T. Tortora, C. C. Almasan, and O. D. Lavrentovich, in *APS Meeting Abstracts*, Vol. 1 (2013) p. 31009.